5

DISCUSSION

This chapter is dedicated to a closer approach to the main result presented in last chapter. Also, it tries to put the results within the frame of already published work, allowing a comparison with other related systems.

Contents

5.1 Properties of CoO/Ag

As presented in the previous chapter, CoO grown on Ag(001) follows an ordered structure, and thus the LEED pattern for the oxide film shows the same intense spots as the substrate. Nevertheless, parameters like oxygen pressure and substrate temperature are playing an important role in growing the CoO(001) layers. Deposition of the oxide using MEED oscillations had been attempted at the beginning of this work, but it seemed impossible to use this technique in our case since the MEED spots of Ag(001) suffer a decay in the intensity due to the heating of the sample and, furthermore, they disappear when the oxygen atmosphere is set in the preparation chamber. The layer-by-layer growth of oxides on different substrates was successfully monitored by means of RHEED [5, 110].

A detailed study of the surface structure of submonolayer islands of CoO on Ag(001) was presented by Sebastian *et al.* [60] and Shantyr *et al.* [44]. They deposited 0.3 ML CoO on Ag(001), and by making use of a low temperature STM and STS (Scanning Tunneling Spectroscopy), they imaged different types of islands. Different kind of oxide formation have been found. They concluded that the different structures are precursors of CoO (NaCl-like structure) or Co_3O_4 (spinel–like structure) [111]. These two precursors were always found together and the ratio between the island surfaces was found to be a function of the substrate temperature. Finally, it was concluded that a higher temperature may lead to the complete formation of a CoO(001) structure. They also addressed the oxygen pressure influence on the growth. Figure 5.1 shows a phase diagram for the CoO/Ag(001) corroborated with own result from the LEED study.

This was reasoned by the argument that a higher oxygen pressure in the deposition chamber ($p \approx 10^{-4}$ mbar) can lead to a CoO(111) type of oxide. The Co_3O_4 structure is a stable surface configuration and can be obtained also from CoO(001) by annealing for several hours at $\approx$ 650 K in oxygen pressure of 10^{-4} mbar [112]. Reports of the formation of spinel structures can be found by van Elp *et al.* for Co_3O_4 obtained from CoO powder annealed at 950 K under oxygen flow [113], and by Mocuta *et al.* [114] reporting that, independent on preparation, polished CoO(111) surface is covered by an epitaxial Co_3O_4 layer.

We turn now our attention to the in-plane structure of the layers. Concerning the LEED patterns recorded from the CoO films, a well-ordered oxide

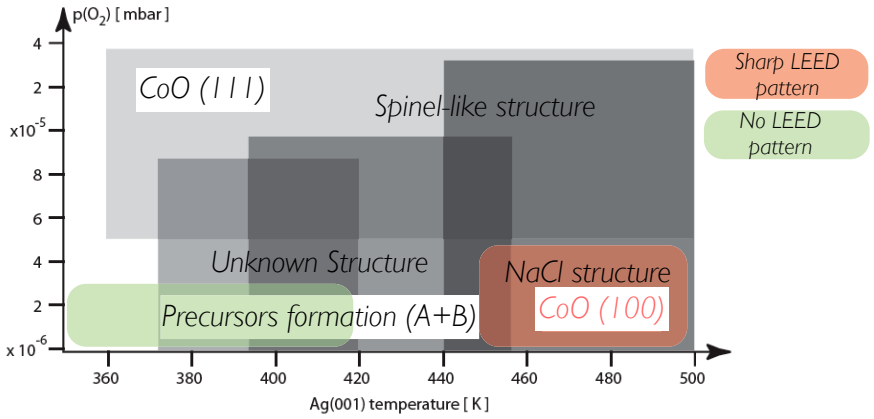

Figure 5.1: Phase diagram of CoO/Ag(001). An increase in the oxygen pressure during evaporation can lead to Co_3O_4 type formation. An increase of the sample temperature during growth avoids precursor formation. The sketch is taken from Ref. [44] and the colored regions represent the studied areas in this work.

structure was observed in the studied range of thickness with no additional superstructure indicating a pseudomorphic growth mode. But nevertheless, a broadening of the spots followed by an increased background was evident.

The *bcc* Fe layer growth on the CoO follows the (001) orientation of the substrate. Important work related to the Fe growth on different types of oxides can be found in Refs. [115, 104, 116]. Figure 5.2 depicts a structure model of the surface plane structure of the Ag substrate (a), CoO (b) and Fe (c) film deposited on top. A 45° rotation of the Fe cubic unit cell (c) matches the lattice constant of the Fe (2.87 Å) to that of the CoO (4.26 Å) and Ag (4.09 Å).

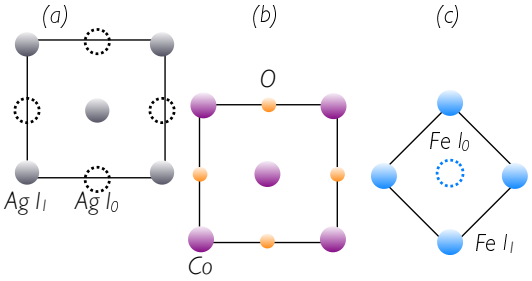

Figure 5.2: Top view of the crystal structure of a rock-salt CoO(001) (b) and *bcc* Fe(001) (c). The Ag(001) substrate (a) is presented for completeness. I_1 (I_0) represents a top (bottom) layer of atoms in the cell.

We will focus now on the lattice. As discussed, the CoO film structure has to accommodate a lateral strain, which results from a lattice mismatch between the bulk phase and the Ag(001) substrate. The lattice mismatch along the in-plane oriented bulk a axis of $(a_{CoO} - a_{Ag})/a_{Ag} = 0.041$ leads to a tensile

strain along ($\bar{1}00$) directions. Thus, the film experiences a compressive in-plane strain. This strain acts indirectly on the film structure normal to the film plane, while the system tends to maintain its atomic volume similar to the bulk. Furthermore, the elastic energy involved in this case has to be reduced by an expansion along the film normal. Our LEED *I(E)* analysis yields an average value of 2.17 $\pm$ 0.03 Å for the vertical interlayer spacing. Twice of this value (4.34 $\pm$ 0.06 Å) gives the out-of-plane lattice constant in the case of CoO/Ag(001). The atomic volume in the case of the vertically distorted CoO film is 72.59 Å^3, 9% reduced compared to the CoO bulk value (77.1 Å^3). The Poisson ratio, calculated as $\nu = -\frac{a_{\perp,film}-a_{\perp,bulk}}{a_{\parallel,film}-a_{\parallel,bulk}}$ between the bulk state and the elongated state, yields a value of 0.47, where $a_{\parallel}$ and $a_{\perp}$ are the values for the in-plane and out-of-plane lattice constant of the distorted and bulk CoO film.

As already presented in Fig. 4.6, a more detailed study of the interlayer spacing of CoO/Ag(001) was made by Wang *et al.* [61] by means of Berbieri – van Hove tensor LEED calculation. The authors have been able to check layer-by-layer vertical spacing in their study yielding different values for each layer depending on the distance to the substrate plane (from 2.40 Å between the Ag and the first oxide layer to 2.25 Å with increasing number of layers, see Fig. 4.6). A lateral strain of the CoO lattice was evaluated to be on the order of 2.88 Å for O–O neighboring atoms leading to a value of 4.07Å for the in-plane lattice constant of the CoO. Csizar *et al.* [5] presented a value of $a = 4.28$ Å for a 90 nm CoO/Ag(001), measuring the out-of-plane spacing by means of X-ray diffraction. This is the indication of a reduced strain in the regime of thick films. In the case of this work, the CoO film is described by an epitaxial growth up to the maximum thickness of 13 ML studied.

The electronic and magnetic properties of CoO thin films change due to the type of strain induced by the substrate. We will focus now on the vertical expansion of the film as demonstrated by LEED *I(E)*. Both types of strain were experimentally used for spectroscopic measurements by Csiszar *et al.* [5] or Haverkort [117] [CoO/Ag(001) for the out-of-plane tetragonal distortion and MnO/CoO/MnO/Ag(001) for the in-plane one].

Figure 5.3 (a) shows the atomic level occupation for the O_h symmetry, which is the proper one for Co surrounded by six oxygen atoms. In this symmetry, the 3*d* atomic levels split in three orbitals with t_{2g} symmetry and two orbitals with e_g symmetry. Two holes are located in the spin-down e_g orbitals

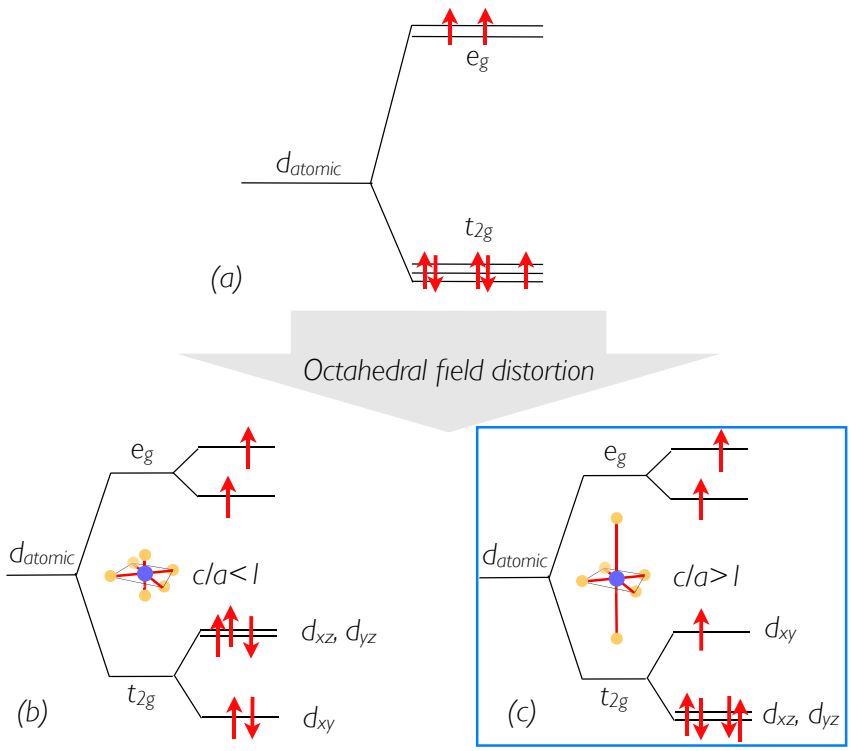

Figure 5.3: Splitting of the atomic levels for Co due to the different distortion of the crystal field. The electronic population of the level is explained in the text [117].

and one hole in the spin-down t_{2g} orbitals for a CoO $3d^7$ high-spin configuration.

Another type of low-energy splitting of the crystal field multiplet is caused by distortions from cubic symmetry. As an example, an elongation of the z-axis lifts the degeneracy of the e_g orbitals, known as the Jahn-Teller effect [118]. The same effect can be also found in the case of the partially occupied t_{2g} orbitals, but with a reduced contribution. Here one should note that the spin-orbit contribution has a larger effect on the t_{2g} states.

Introducing a structural distortion in our system, we will force the t_{2g} levels to split. Now the discussion regards the magnitude of the splitting compared to the spin-orbit interaction.

- **CoO film with tensile in-plane strain ($c/a < 1$)**

  For this distortion, the d_{xy} orbital is lower in energy than the d_{xz} and d_{yx} and their degeneracy is removed. This description suits the case where the splitting is much larger than the spin-orbit interaction, thus the t_{2g}

hole can be located on the linear combination of d_{xz} and d_{yz} orbitals, $d_1 = \sqrt{\frac{1}{2}}(-d_{xz} - id_{yz})$. By using the d_{xz} and the d_{yz} orbitals only an orbital moment in the z direction can be created and not in the x or y directions. So, finally a state with $m_l = -1$ is produced, *i.e.* a state having an orbital moment perpendicular to the film surface. Now, considering that the spin of an electron for a TM belonging to the 2^{nd} half of the series wants to align anti-parallel to its orbital moment, one can conclude that also an out-of-plane spin direction occurs.

- **CoO film with compressive in-plane strain ($c/a > 1$).** This is the case for the studied system Fe/CoO/Ag(001).

  Due to the tetragonal distortion, leading in this case to a different overlap between the Co d_{xy} and oxygen orbitals on the vertical, the energy level for d_{xy} will be higher than for the d_{zx} and d_{yz}. In this case the splitting of the t_{2g} levels is different in such a way that the hole will be located in the d_{xy} orbital, which results in a final state with a quenched orbital moment (the spin is free to orient to any direction) [119]. But, in reality, the idea behind is that even though the c/a is, in this case, bigger than unity, it is only slightly. Thus, the system is in an "intermediate" state, with the t_{2g} splitting smaller than the spin-orbit interaction. As a result, the orbital moment is not fully quenched [117], and furthermore, there is an in-plane orbital moment and thus the preferred spin direction should be in the film plane.

Since the vertical expansion of the CoO film presented in Sect. 4.1 has strong implications for the electronic, and thus, the magnetic structure of the oxide, it is good to remember here the bulk spin structure of the CoO which is presented in Fig. 5.4. Like NiO, FeO, and MnO, the CoO is a type-II antiferromagnet, meaning that the spins situated in {111} planes are parallel, each neighbor plane being antiparallelly aligned. The easy direction of moments is along $\{11\bar{2}\}$ for MnO and NiO, along [111] directions in the FeO and at an angle of 27.4° from [001] in the (111) planes for CoO [42]. As mentioned, the CoO bulk experiences a tetragonal crystallographic distortion (1.2%) in the ordered magnetic state. Mocuta *et al.* [46] argue that the spins do not lie in the (111) planes, but are parallel to a $[\bar{1}\bar{1}7]$ direction: the spins are tilted 23.8° above the (111) plane and 11.4° from the [001] contraction axis.

The case of the bulk CoO ($a/c = 1$ in the previous notation) has to be con-

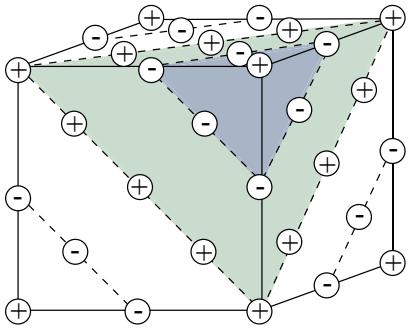

Figure 5.4: Magnetic unit cell of bulk CoO. Positive and negative signs refer to the oppositely directed moments on the cations, and the oxygen ions are omitted from the diagram since they carry no magnetic information [42].

sidered as starting point for our discussion. The spin structure corresponding to the bulk CoO changes drastically to an in-plane or out-of-plane spin structure depending on the kind of distortion that the film suffers. Considering a simple model of the spin structure presented in Figs. 5.4 and 2.8, the spin axis of the bulk would "fall" (in the case of a vertical distorted CoO film) into the sample plane and would be energetically most favorable along the [110] directions. Our results from XMLD measurements for Fe/CoO/Ag(001) are consistent with this assumption.

Our study is addressing the vertical expansion of the 10 ML CoO/Ag(001) by means of XAS (Fig. 4.10). The huge dichroism (see the normal minus grazing spectra) found in this case is attributed to this deformation. At normal incidence, one probes with horizontal linearly polarized light a perfect rectangular grid of atomic orbitals within a fourfold symmetry. Thus, a 90° rotation of the sample within the surface plane or of the **E** vector should not be visible in the absorption spectra. Now, going to grazing incidence, for a perfect cubic symmetry, the spectra should resemble the normal incidence ones (small differences might occur taking into account the impossibility to measure at maximum grazing angle). Considering our vertical distortion out-of-plane, this will cause a distortion of the orbitals along the vertical direction. Thus, the horizontal light will probe now orbitals elongated along the **E** vector direction.

This large crystal structure effect found for non-normal incidence absorption spectroscopy is a challenge when measuring the magnetic linear dichroism in this geometry because the signal is about ten times bigger than the magnetic signal and it is superimposed to the latter one in all the spectral features of the Co $L_{2,3}$ edge. On the other hand, for the normal incidence measurements geometry, the absence of the dichroic signal above T_{AFM} is evident in Fig. 4.10 (b). Nevertheless, this geometry was suitable for our study, taking also into account

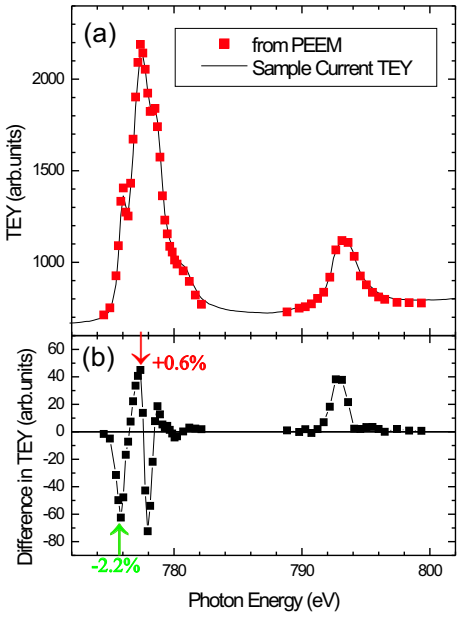

Figure 5.5: XMLD measured for 8 Ml CoO/NiO by means of PEEM (red dots, representing the asymmetry for each energy) and by XAS total electron yield (solid line) [107].

the expected in-plane orientation of the spin axis in the case of a vertically expanded CoO film. In this case, it would have been difficult to determine an out-of-plane component of the spin axis, because the magnetic signal measured from a polar dependence of the XMLD signal, would have been superimposed onto a structural contribution in all the spectral features of the L_3 edge. Furthermore, a much larger signal than the magnetic one is coming from the structural dichroism, thus making it harder to separate the two contributions to the XMLD signal, as presented in Fig. 4.14.

The CoO/Ag(001) spectra from Refs. [5, 110] were measured in a special geometry, with the sample tilted with respect to the incoming beam, and the change in the polarization was made by rotating the sample around the Poynting vector axis, which made a 70° angle with respect to the sample normal. Because of this measurement geometry, one can not directly compare the published spectra and the ones presented in this work. In the geometry used in the references, for the spectra measured at 77 K , there is an interplay of magnetic and structural contribution to the overall XMLD signal, on the other hand, we present in this work mainly magnetic XMLD spectra. But, nevertheless, a comparison concerning the spectral shape of the XAS spectra is possible for the one measured at grazing incidence (Fig. 4.10) and it shows the structural contribution to the overall XMLD signal.

We are now turning our attention to the Fe/CoO bilayers. The XMLD signal measured at 150 K after depositing the Fe layer on top of the CoO, shows a pronounced dichroic signal. The geometry was kept such that no structural dichroism was detected. The spectral features and the XMLD lineshapes of Figs. 4.14 and 4.16 are in good agreement with spectra of N. Weber for 8 ML CoO/NiO [107], measured by means of XAS and PEEM. The spectra in Fig. 5.5 were measured on 8 ML CoO deposited *in-situ* on bulk NiO by reactive co-deposition of Co and O.

5.2 Closer look at the Fe/CoO interface

This section is dedicated to the effects that occur at the FM/antiferromagnetic oxide interface, namely the induced magnetic moments in the antiferromagnet and the oxidation of the FM.

5.2.1 Interfacial induced magnetic moments

Our investigation of the magnetic (domain) structure in Fe/CoO/Ag(001) systems by XAS and XMCD-PEEM revealed the presence of a small ferromagnetic net moment when measuring at the Co $L_{2,3}$ edges. It was surprising that the signal was present at 150 K, as well at room temperature. From the vanishing signal for a pure CoO/Ag(001) film and the coinciding magnetic domain patterns in Co and Fe PEEM images recorded on Fe/CoO bilayers, it was concluded that the Fe layer is inducing some ferromagnetic order in the CoO. Furthermore, there is no connection to the antiferromagnetism of the CoO since the XMCD signal was also visible when the oxide was in a paramagnetic state.

Even though the depth-profiling is not one of the features of the XMCD-PEEM, one can estimate the density of ferromagnetic moments situated at the interface. Calculating the asymmetry defined as $\frac{\mu^+_{L_3}-\mu^-_{L_3}}{\mu^+_{L_3}+\mu^-_{L_3}}$ for XMCD at the Co L_3 edge for 6 ML Fe/10 ML CoO and for 10 ML Co/Cu(001) values of 3% and 18% are obtained, where $\mu^+_{L_3}$ and $\mu^-_{L_3}$ are the maximum Co XMCD L_3 signal for both circular polarization. Now, the question raises how many MLs of interfacial spins contribute to the Co XMCD signal. For this, we have assumed that all ferromagnetic spins in CoO are localized at the interface and have the same ori-

entation and the same magnetic moment as the Co metallic film. Furthermore, an electron yield information depth of $\lambda = 2$ nm was assumed [19].

$$\frac{XMCD(\mathrm{CoO})}{XMCD(\mathrm{Co})} = \frac{3\%}{18\%} = \frac{1 + xe^{1/\lambda}}{\sum_{n=0}^{9} e^{-n/\lambda}} \tag{5.1}$$

From Eq. 5.1 (valid for the case when more than 1 ML and less than 2 ML contribute to the signal), one can extract the x value representing the fraction of the second monolayer yielding ferromagnetic signal. 10 ML are involved in the calculation starting from 0 ML for the Fe interface to 9 ML for the CoO/Ag(001) interface. This yields a value of $x = 0.11$, thus 1.1 ($\pm$0.2) ML CoO are ferromagnetically aligned at the interface. Here one should stress that this value is just a rough estimate, valid only under the simplified assumption mentioned before. The amount of affected CoO material would be much higher if one assumes a smaller effective magnetic moment per atom. However, similar values were found by Ohldag *et al.* [108] for a Co/NiO system measured by XAS and PEEM. They concluded that 0.75 ML of Ni or 1.5 ML of $CoNiO_x$ give rise to the interfacial spin polarization.

From the PEEM study (Fig. 4.24), it is evident that the ferromagnetic domains in the CoO layer reveal the same number of different contrast levels as the Fe domains. The spatial distribution of the domains for Co is a complete replica of the ferromagnetic Fe domain pattern. This demonstrates a ferromagnetic alignment between the Fe and ferromagnetic Co at the interface. The coupling is similar at room temperature and at 170 K. The spectroscopic measurements on Fe/CoO/Ag(001) described in this work prove the same orientation for the XMCD in the CoO by looking at the maximum of the XMCD signal recorded for different angles.

Radu *et al.* [6, 62] described the same effect for sputter-deposited 25 Å CoO/ 150 Å Fe films. Soft X-ray magnetic scattering and element-specific hysteresis loops were used to address separately each layer. The non-vanishing magnetic dichroic signal for Co was seen for all temperatures, above and below the CoO ordering temperature. An in-phase reversal of the hysteresis loops was seen, but the coercive field is different. The authors concluded that a part of the interfacial spins are "free" to rotate when rotating the ferromagnetic layer because they are coupled to it. Another part of the spins are "frozen", being

strongly coupled to the antiferromagnet itself. No estimation of the number of the magnetic moments for the both cases was presented.

By using XMCD-PEEM, induced magnetic moments in Fe and Mn were imaged also by Offi *et al.* [120] in Co/FeMn bilayers. They concluded that 30% of the total interfacial Fe moments is aligned to the Co magnetization in the system. For the Mn, due to the low magnetic signal, it was impossible to separate the part strongly coupled to the AFM layer from the one free to rotate with the Co. Also for this system, the uncompensated moments were present above and below T_{AFM} of the antiferromagnet.

Here it is worth to discuss the more recent work of Ohldag *et al.* [121], which proved a direct correlation between the pinned interfacial spins and the rotatable ones. At the interface, two types of spins can be found: the pinned moments are more fixed at the interface and coupled to the AFM layer, whereas the rotatable moments are coupled to the FM and can rotate when the magnetization direction in the ferromagnet is changed. Element-specific hysteresis loops showed a horizontal loop shift, as expected in EB systems, but also a vertical loop shift caused by the pinned magnetic moments. Finally they concluded that 4% of the interfacial layers contains *pinned* spins. In contradiction to the idea of pinned moments at the interface, a depth profile study by Roy *et al.* [122] showed that the Fe uncompensated interfacial moments in Co/FeF_2 follow the Co moments in an antiparallel manner, while uncompensated moments that are not at the interface stay fixed in their pinned positions during the magnetization reversal.

Many studies of different systems have as outcome the evidence of ferromagnetic induced moments at the interface. All transition metals can be enumerated here: Rh/Fe(001) [123], Fe/V [124], Fe/Cu [125], Co/Cu [125, 126], to name only a few. They were observed at the interface between a metal and an oxide Fe/NiO, Co/NiO, Py/CoO, Fe/CoO [4, 108], etc. Recently, this effect was also found to occur at the FM/semiconductor interface Fe/Ge [127].

In the case of a single CoO film, our XMCD measurements at the Co L_{23} edges after magnetically saturating the film, lead to zero signal. As we already suggested, this can be the indication that there are no random spin-clusters with ferromagnetic behavior in our film volume. But, nevertheless, a pure CoO XMCD spectrum can be recorded if high enough external fields are used to induce a magnetic order. Figure 5.6 reproduced from Ref. [117] shows

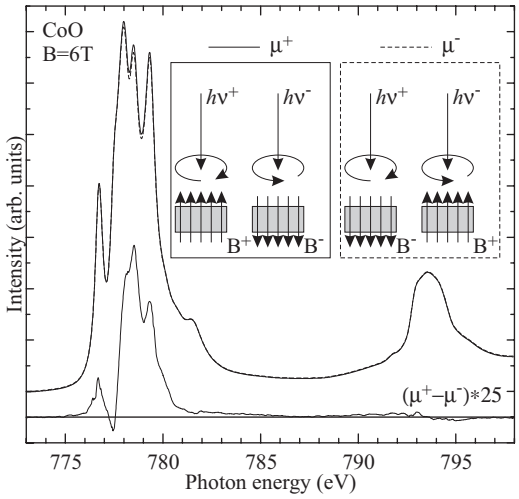

Figure 5.6: Circular dichroism of bulk CoO in the paramagnetic state at 291 K under an external magnetic field of 6 T. The circular dichroism arises due to the induced magnetic moments by the magnetic field. (taken from Ref. [117])

the XMCD signal recorded for bulk CoO in the paramagnetic phase at 290 K, at the Co $L_{2,3}$ edges, for normal incidence an in a field of 6 T. A quantitatively analysis of the XAS spectra presented in the figure reveals an asymmetry value of 1.2%. The calculated 3% for the interfacial spins confirm a much higher exchange coupling at the interface for the Fe/CoO system. The orbital moment found for CoO is surprisingly large but in accordance with the cluster calculation performed by the same group.

The XMCD signal presented in Fig. 4.19 resembles the one shown in Fig. 5.6. One should stress here that the small features visible in the L_3 XMCD signal for CoO (Fig. 4.19) are *not* related to measurement noise. Note that the line profile of the XMCD signal is replicating all the features of the XAS spectra, indicating that the uncompensated Co spins retain their oxide character. In the recent work of Braicovich *et al.* [128] on Co-ferrite ($CoFe_2O_4$), the same effect was detected from measurements by circular dichroism at the Co $L_{2,3}$ edges. The XMCD signal was found in all the spectral features of the $L_{2,3}$ edges. It is good to remember here the line shape of the XMCD signal for metallic Co, showing only two broad peaks at the $L_{2,3}$ edges (Fig. 4.19).

5.2.2 Interfacial Fe oxidation

It was shown in Sect. 4.3.3 that the Co at the interface is influenced by the ferromagnetic Fe on top. We will now follow how the Fe layer is influenced by the oxide. The effect of the oxidation at the interface was already introduced

in Chapter 4, in which a detailed study on the fractions of monolayer was presented, and it revealed an XAS spectrum measured at the Fe $L_{2,3}$ edges characterized by oxidic spectral features.

The inset of Fig. 4.18 depicts the XAS spectra recorded for a fraction of a monolayer of Fe deposited on CoO. The arrows in the figure indicate the oxide spectral features. To explain the oxide formation, chemical forces need to be considered. The electronegativity is a measure of a particular material to attract electrons. The reversed measure of the electronegativity is the reduction potential. Respective values of electronegativity (reduction) for Fe and Co are 1.6(-0.47) and 1.7(-0.27) V [108]. From this elemental data, it can be concluded that Fe can reduce CoO when they are in contact. For the investigation of the oxide formed at the interface, the measured spectra were compared with literature spectra measured for different Fe oxide types. Figure 5.7 presents the XAS spectra for most common Fe oxides. It is evident that Fe_3O_4 and Fe_2O_3 can be excluded from the discussion due to their L_3 edge shape and their L_3 energy shift, which is clearly different from metallic Fe or FeO type. Furthermore, the pre-edge of the spectra can be a good indication of the type of oxide formation, the features found for the FeO spectrum cannot be found in the other spectra. The measured shifts in energy of the L_3 peak from the "initial" metallic value are ~ 0 eV (FeO), ~ 1.4 eV (Fe_3O_4), ~ 1.7 eV (Fe_2O_3) [4]. Our measured Fe XAS spectra resemble accurately the FeO type. If one assumes also a Fe_3O_4 or Fe_2O_3 oxide formation in parallel, their amount would be significantly smaller than the amount of FeO and maybe not visible in the absorption spectrum. Experiments of Fe oxidation in the presence of different pressures of oxygen lead to the conclusion that the formation of the lower oxide, the compound FeO, occurs when oxygen is available in limited quantities. Results from *ex-situ* grown 10 Å CoO/ 10 Å Fe [109] predict ≈ 5 ML of interfacial mixing but the separation of a pure metallic and a mono oxide spectra seemed to be a challenge.

Redox effects between metals and oxides have been intensively studied because of the antiferromagnetic character of the oxide layers. One of the most detailed works involved Fe/NiO and NiO/Fe studied by XAS [4, 109, 129] or XPS [130]. The oxide layer thickness at the interface depends on the growth sequence of the Fe and NiO layers. For 20 ML NiO on top of bulk Fe(001), a 19 Å thick Fe_3O_4 layer is produced at the interface [129]. On the other hand, if Fe is deposited on top of NiO, only a 3 ML thick intermixed layer is formed. That was the idea that stood behind in choosing the latter alternative for growing the

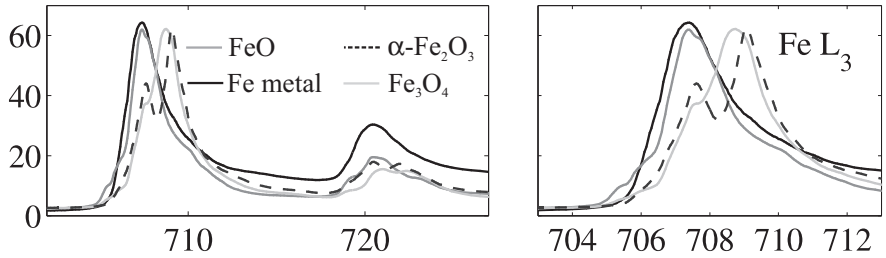

Figure 5.7: Different types of Fe oxide. Metallic and FeO show the same energy maximum at the L_3 but Fe_3O_4 and Fe_2O_3 show a shift in energy for the L_3 maximum. The graphs are from Ref. [109].

samples studied in this work.

As expected, the annealing temperature plays an important role for the quality of the interface. This effect was pictured by Regan *et al.* [4] by means of XAS at Co $L_{2,3}$ for a MgO(001)/NiO (600 Å)/CoO (10Å)/Fe (15Å)/Ru multilayer structure. The increased reduction of CoO after annealing is visible in a lessening of the multiplet structure, but also in a reduction of the L_3 intensity.

For NiO/Fe, a sample annealing after the deposition, can destroy the NiO overlayer. The nickel atoms were found to "dissolve" into the substrate yielding to the formation of an Fe oxide layer similar to FeO [129].

An estimation of the amount of FeO formed at the interface was done using the model described in Ref. [109] and yielded a value of 0.3 ML of Fe oxidized at the interface. Larger oxidation effects of Fe/NiO compared to Fe/CoO are understandable because of the different oxidation–reduction factors of Ni and Co. The interface quality is also playing an important role in the oxide formation. Recently, Luches *et al.* [131] presented a model for the Fe/NiO interface, suggesting that an Fe–Ni alloy is formed on top of interfacial FeO. In this case, the FeO suffers a lattice vertical distortion at the interface of 7% and a 0.3 Å buckling in the Fe and O atomic positions, this being the reason of an increase of the spin magnetic moment of the Fe by 0.6 μ_B. A two-dimensional FeO layer has also been observed at the MgO/Fe(001) interface by Meyerheim *et al.* [132]. Tusche *et al.* [133] predicted the formation of a CoNiO interfacial layer between the Co and NiO due to a crystallographic reconstruction of the interface.

Less oxidation/reduction effects are evident for Fe/CoO/Ag(001) in comparison to the previously cited work. A reduction of the effect is a direct consequence of the elctronegativity/reduction potential for both two species.

NiO (electronegativity/reduction potential for Ni is 1.8/-0.23 V), in comparison to CoO, is easier to get reduced by the Fe. Less interfacial oxidation effects can also be a direct consequence of the high quality of the interface, hence of the deposited layers. As already suggested in Chapter 4, CoO shows an ordered growth mode and furthermore, the Fe layer atop was deposited at room temperature and no further annealing was carried out. The absence of the annealing after preparing the bilayers can indeed reduce the quality of the surface of the Fe deposited on top (less sharp spots in LEED patterns of Fig. 4.4 are visible), but nevertheless, it will reduce the oxidation effect due to the diffusion of O from the CoO to the Fe layer.

Another problem that should be discussed here is the amount of Co moments contributing to the XMCD signal at the Co $L_{2,3}$ edges. Due to the oxidation of the Fe (0.3 ML) at the contact interface with CoO, a part of the Co is reduced, as already shown before. But, the Co-XMCD signal recorded shows prominent oxide features in the line shape, that made us deduce that the Co keeps its oxide character and is coupled to the ferromagnetic Fe layer. The overall XMCD signal from interfacial uncompensated Co spins contains two parts. One is the oxidized Co signal (as expected in an CoO film) and the other one could be a metallic Co signal (coming from the reduced Co due to the redox effects). Both parts contribute to the total measured XMCD but the metallic and oxidic features in the XAS spectra are superimposed, thus making it impossible to distinguish them. Here one should stress, as mentioned before, that the amount of interfacial spins can be related to the magnitude of the exchange-bias effect, hence with the interfacial magnetic coupling [19, 108]. Furthermore, a small oxidation/reduction effect does *not* imply a reduced number of interfacial spins, because, as deduced from the experiments, the Co atoms keep their oxidation state and nevertheless can be ferromagnetically coupled to the Fe layer.

5.2.3 FM/AFM magnetic interlayer coupling

After regarding the interface from a chemical and a magnetic points of view and introducing the coupling *via* the uncompensated Co spin moments, we now turn our attention to the magnetic interlayer coupling.

From the fit of the Fe XMCD at 300 K, a $\phi_{Fe}(RT) = 44.3^{\circ}$ angle between $\mathbf{M}_{Fe}$ and the [100] axis is obtained. After zero-field cooling, the Fe magnetic

easy direction is kept [$\phi_{Fe}(LT) = 42.5°$], agreeing within the error bar with the MOKE results described in Sect. 4.2.

The small decrease in the Fe L_3 XMCD intensities observed upon cooling can be explained by a partial breaking-up into domains or by a canting or *fanning* [66] of the Fe magnetization concomitant to the development of the CoO antiferromagnetic order. The preferential orientation of the Fe moments in Fe/CoO/Ag(001) along one of the $\langle 110 \rangle$ directions may suffer small local twists of the Fe moments into the direction defined by the adjacent Co moments. These small twists towards the lateral $\langle 100 \rangle$ or $\langle 010 \rangle$ directions would lead to an exchange interaction-induced modulation of the Fe magnetization within one domain. This so-called fanning of the magnetization would result in a reduction of the domain-averaged XMCD asymmetry. The asymmetry calculated from the PEEM images for larger domains shows a higher value than the one calculated averaging over a small domain. However, this is not a clear proof for fanning since the small domain size is close to the instrument resolution.

From a qualitative examination of XMCD and XMLD PEEM images, the contrast clearly reveals a collinear coupling between the antiferromagnetic axis of the domains and the ferromagnetic directions in the Fe layer. No rotation of the Fe magnetization was visible from the Fe XMCD images recorded at room temperature and at 170 K.

A PEEM study of Co/FeMn [134, 135] and Co/NiMn [66] structures reveals this kind of rotation. In this system, the Co moments were found to rotate by 45° from $\langle 110 \rangle$ to $\langle 100 \rangle$ directions as the FeMn film undergoes the magnetic phase transition from para- to antiferromagnetic at a certain thickness. The rotation of the Co moments could be explained by assuming a bulk-like 3Q spin structure in the FeMn film, as presented by Kuch *et al.* [20]. The non-collinear 3Q spin structure of FeMn gives rise to topological 90° domains at the AFM interface. The Co/FeMn interface is characterised by fully compensated 90° domains with spin axes pointing along $\langle 110 \rangle$ directions and a different net moment resulting from the uncompensated moments at the step edges. This surface spin structure favours a net coupling at intermediate 45° directions along $\langle 100 \rangle$ directions [134]. In the case of Fe/CoO bilayers, the magnetization direction of the Fe follows, as mentioned before, the $\langle 110 \rangle$ directions of the substrate. Considering now that the spin axis of the CoO this film, reporting to the bulk spin axis, will be in-plane, the most energetically favorable orientation would

be also the $\langle 110 \rangle$ directions. Thus the most stable state of the system is fulfilled with both Fe magnetization and Co spin axis aligned along the same crystallographic direction.

Ohldag *et al.* [19, 108] showed a collinear coupling between the spin axis of each antiferromagnetic domain and the uniaxial anisotropy of adjacent ferromagnetic domains in the case of Fe and Co deposited on NiO(001). The quantitative analysis yields a common preferred axis of the two magnetic systems which is parallel to [110]. It was also found that the antiferromagnet experiences an in-plane reorientation after depositing the ferromagnetic material on top. The antiferromagnetic configuration at the buried (001) surface resembles the one of an antiferromagnetic domain wall parallel to the interface.

Reviewing the Co/NiO system, a very recent paper by Arenholz *et al.* [136] put the magnetic coupling between the two layers in a different light. The argument is that there is a dependence of the XMLD spectra on the relative orientations of the crystallographic directions, the spin axis of the antiferromagnet and the electric field vector **E** of the linearly polarized incoming light. In a system with octahedral ligand field symmetry, any XMLD spectrum can be formed by a linear combination of two fundamental spectra I_0 and I_{45}, not just one as it was previously used [137]. These spectra were obtained by making use of atomic multiplet calculations [138].

They represent the XMLD signal observed as the difference of the spectra with **E** parallel and perpendicular to **M**, for $\mathbf{M} \parallel [100]$ (I_0) and $\mathbf{M} \parallel [110]$ (I_{45}). In particular, it was found that the XMLD signal at the Ni L_2 edge reverses sign when the AFM spin axis of the NiO is turned from $\langle 100 \rangle$ to $\langle 110 \rangle$ crystallographic directions. Finally, it was concluded that the coupling between the Co and NiO layers is perpendicular, in contrast to the previous publication [19]. In our case, it is observed that the Co spin axis in the CoO layer below T_{AFM} is along the $\langle 110 \rangle$ directions, either parallel or perpendicular to the $\mathbf{M}_{Fe}$ direction, but in any case, describable by I_{45}.

When measuring the Co $L_{2,3}$ XMLD defined as stated above, we obtain a negative-positive-negative peak structure at the L_3 edge and a mainly positive peak at the L_2 edge. It is now very important to find out the correct sign of the XMLD in order to determine whether the coupling between the CoO spin axis and $\mathbf{M}_{Fe}$ is parallel or perpendicular. Unfortunately, up to this date, they are no calculations available of I_{45} for the CoO case. On the other hand, I_0 can be

found in Ref. [106].

If we focus on the I_0 spectrum shown in Fig. 2 of Ref. [136], we observe that it fully agrees with the calculated spectrum for the Ni case as presented in Fig. 1(h) of Ref. [106] for $z = 1$ and $\Delta = 1$, where z is the scaling factor of the $3d$ spin-orbit interactions and $\Delta = 10$Dq is the strength parameter of the octahedral crystal field. This is consistent since all the calculated spectra in Ref. [106] are for a [100] spin axis. Measurements and calculations show a sign reversal between I_0 and I_{45} at the Ni L_2 edge.

At the same time, the calculated spectrum for Co, with the same parameters as mentioned above [see Fig. 1(g) in Ref. [106]], shows a complicated peak structure at the L_3 edge, and a mainly negative feature at the L_2. According to our notation, this spectrum is I_0 in the case of CoO.

Analogous calculations for Mn^{2+}[139] and Fe^{2+} [140] exist and they show exactly the same sign reversal at the L_2 edge between I_0 and I_{45}. In order to determine the spin axis in the case of Fe/CoO bilayers, it is assumed that the same sign reversal between I_0 and I_{45} at the Co-L_2 edge occurs. If we now recall the negative L_2 peak found at the I_0 spectrum for Co from Ref. [106], we infer that I_{45} will show a positive peak at the L_2 edge.

By comparing this result with the positive Co L_2 feature displayed by our Co $L_{2,3}$ XMLD spectrum (see Fig. 4.16), we conclude that the coupling between the Fe and the CoO is a parallel one.

This approach is consistent to the previously mentioned published data and we strongly believe that will be supported by reliable calculations in the near future.

For an compensated spin surface of the CoO as presented in Fig. 5.4, a parallel coupling between Fe and CoO can be explained by considering the large amount of interfacial uncompensated Co spins measured the interface.